Supporting Information

Rationally Tuning Host-guest Interactions to Free Hydroxide Ions within Intertrimerically Cuprophic Metal-organic Frameworks for High OH^- Conductivity

Ziyin Li,[1] Zhangjing Zhang,[1,2*] Yingxiang Ye,[1] Kaicong Cai,[1] Fenfen Du,[1] Heng Zeng,[1] Jin Tao,[1] Quanjie Lin,[1] Ying Zheng[1] & Shengchang Xiang[1,2*]

[1]*College of Materials Science and Engineering, Fujian Provincial Key Laboratory of Polymer Materials, Fujian Normal University, 32 Shangsan Road, Fuzhou 350007, China*

[2]*State Key Laboratory of Structural Chemistry, Fujian Institute of Research on the Structure of Matter, Chinese Academy of Sciences, Fuzhou, Fujian 350002, PR China*

E-mail: zzhang@fjnu.edu.cn; scxiang@fjnu.edu.cn

Content

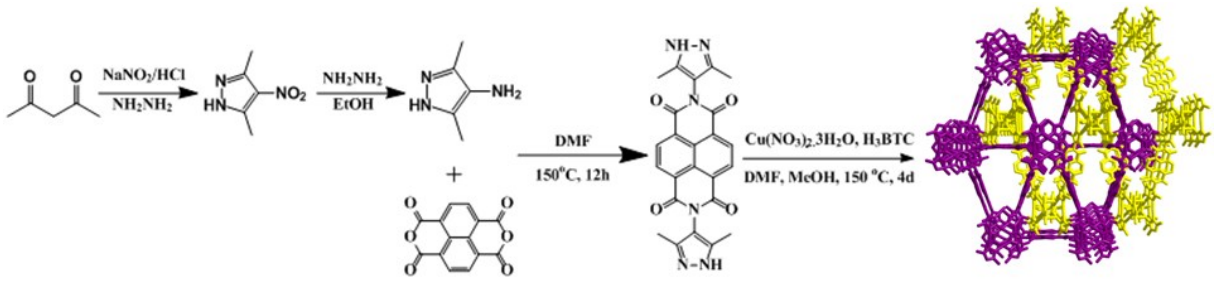

Scheme S1 | Schematic representation of synthesis of **FJU-66·S**.

Synthesis of 4-amine-3,5-dimethyl-1H-pyrazole. This was prepared as described previously.[1] The acetylacetone (20 g, 0.2 mol) was added to the solution of concentrated HCl (18 mL, 0.6 mol) and deionized water (100 mL, 5.55 mol), then stir in the ice water bath (8 ^{o}C). Sodium nitrite solution (14 g, 0.2 mol) was drop into the above solution, standing for 20 min. Opening electric stirring, 85% hydrazine hydrate (12 g, 0.2 mol) was added to reaction which will form a large number of blue recipitate. Continue adding ethanol (100 mL, 2.6 mol) till the blue precipitate were dissolved completely, then adjusted the pH to neutral. Hydrazine hydrate (13.5 g, 0.22 mol) was added dropwise to the above solution, maintaining the temperature at 80 ^{o}C for 5 h until the solution of reaction turned golden yellow. Finally, the solvent was evaporated and the desired product was washed with cold ethanol for three times, then collected by filtration and dried in 60 ^{o}C to afford white powders. (Yield 50.6% based on acetylacetone).

Synthesis of H_2NDI. H_2NDI were prepared as described previously with some modification.[2] A dry 100 mL Schlenk flask was charged with 1,4,5,8-naphthalenetetracarboxylicdianhydride (0.86 g, 3.2 mmol), 3,5-dimethylpyrazole (0.75 g, 6.8 mmol), and anhydrous DMF (50 mL) under a nitrogen atmosphere. The reaction mixture was heated at 150 ^{o}C with rapid stirring for 12 hours. The flask was cooled to room temperature and the dark brown DMF solution was poured into stirring diethyl ether (150 mL). The precipitated yellow solid was separated by filtration and recrystallized from DMF/diethyl ether/H_2O (10 mL: 15 mL: 5 mL). The product was filtered and dried *in vacuo*at 70 ^{o}C to afford 1.2 g (Yield 82% based on 1,4,5,8-naphthalenetetracarboxylicdianhydride) of light yellow crystals. H_2NDI crystallizes in the triclinic crystal system within space group *P-1*, a = 8.955 (1) Å, b = 9.741 (1) Å, c=9.849 (2) Å, α = 110.18 (3), β = 100.69 (3), γ = 93.05 (3), V = 786.010 (4) Å^3.

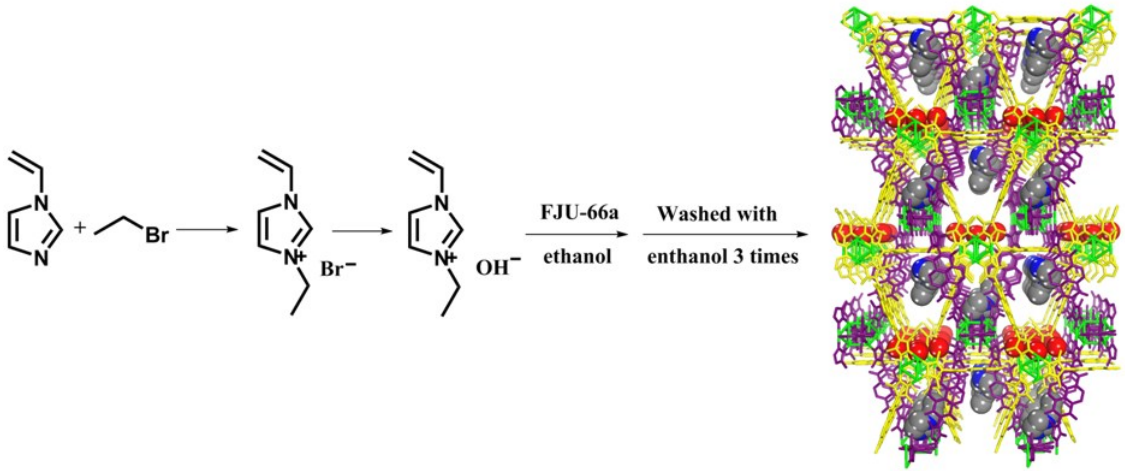

Scheme S2 | Schematic representation of synthesis of **FJU-66·[EVIm]OH**.

Synthesis of 1-ethyl-3-vinylimidazolium bromide ([EVIm]Br). Bromoethane (14 g, 0.128 mol) was added to a solution of 1-vinylimidazole (9 g, 0.096 mol), the mixture was stirred at 80 ^{o}C for 6 h. The pale yellow solid was obtained, then washed with an excess of ethyl ether and dried in *vacuo* at 60 ^{o}C for 24 h. ^{1}H NMR (400 MHz; D_2O): δ9.06 (s, 1H, -N-C*H*-N-), δ 7.77 (d, 1H, -N-C*H*-CH-N-), δ 7.60 (1H, d, -N-C*H*-CH-N-), δ7.15 (1H, dd, CH_2=C*H*), δ5.81 (1H, dd, CH_2=CH), δ5.43 (1H, dd, CH_2=CH), δ4.29 (2H, qd, -N-CH_2-CH_3), δ1.54 (3H, tp, -N-CH_2-CH_3).

Synthesis of 1-ethyl-3-vinylimidazolium hydroxide ([EVIm]OH). VBr was dissolved in ethanol and the solution was added slowly to KOH (1.5 times of VBr molar) solution in ethanol while stirring vigorously. White precipitate was generated and filtered. The filtrate was harvested as [EVIm]OH solution in ethanol. ^{1}H NMR (400 MHz; D_2O): δ 9.79 (s, 1H, -N-C*H*-N-), δ 8.20 (d, 1H, -N-C*H*-CH-N-), δ 7.52 (1H, d, -N-C*H*-CH-N-), δ 6.99 (1H, dd, CH_2=C*H*), δ 5.32 (1H, dd, CH_2=CH), δ 5.16 (1H, dd, CH_2=CH), δ 3.65 (2H, qd, -N-CH_2-CH_3) δ1.15 (3H, tp, -N-CH_2-CH_3).

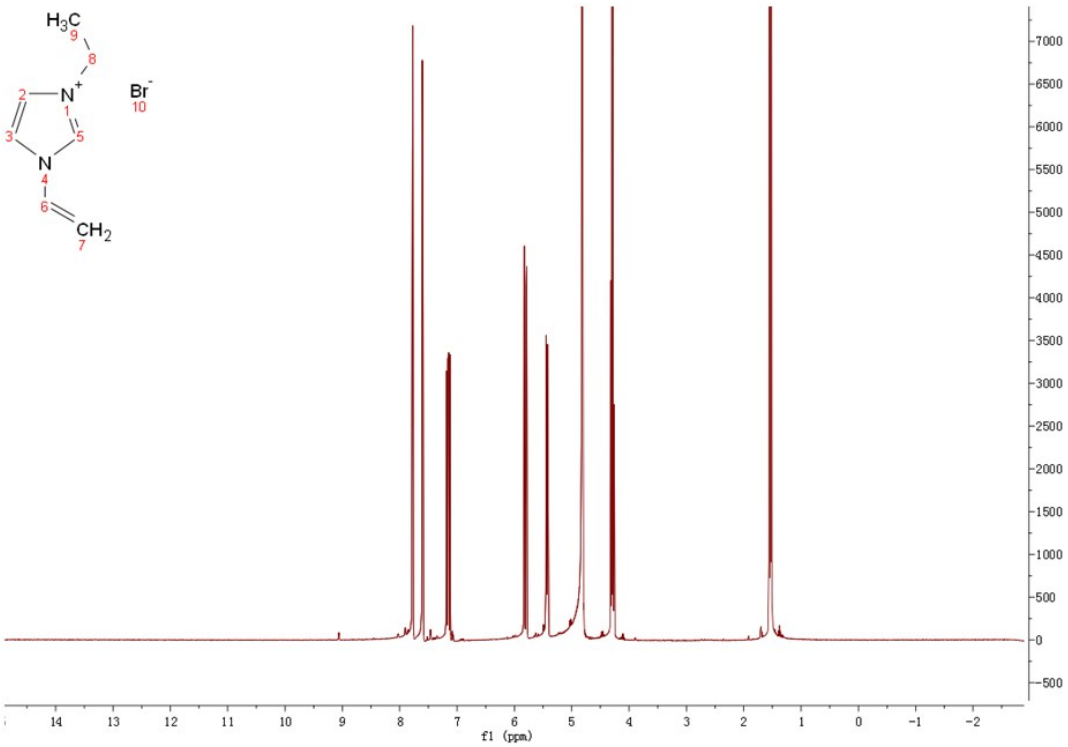

Figure S1 | ^{1}H NMR spectra of [EVIm]Br (D_2O, 400 MHz).

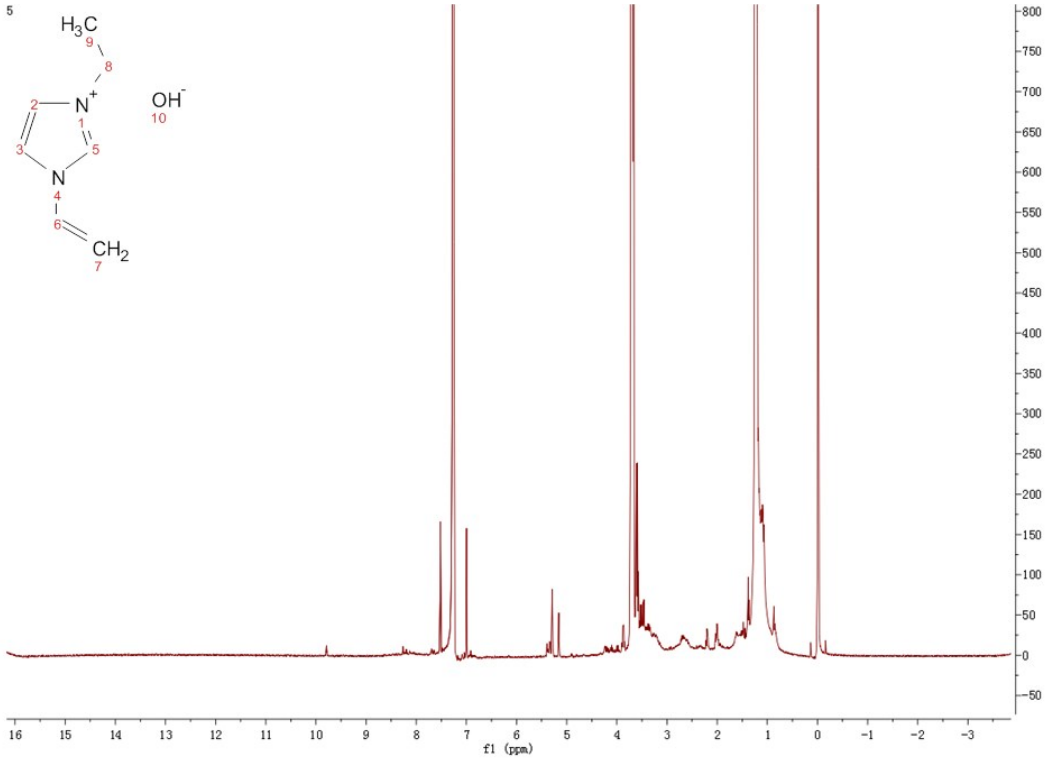

Figure S2 | ^{1}H NMR spectra of [EVIm]OH (D_2O, 400 MHz).

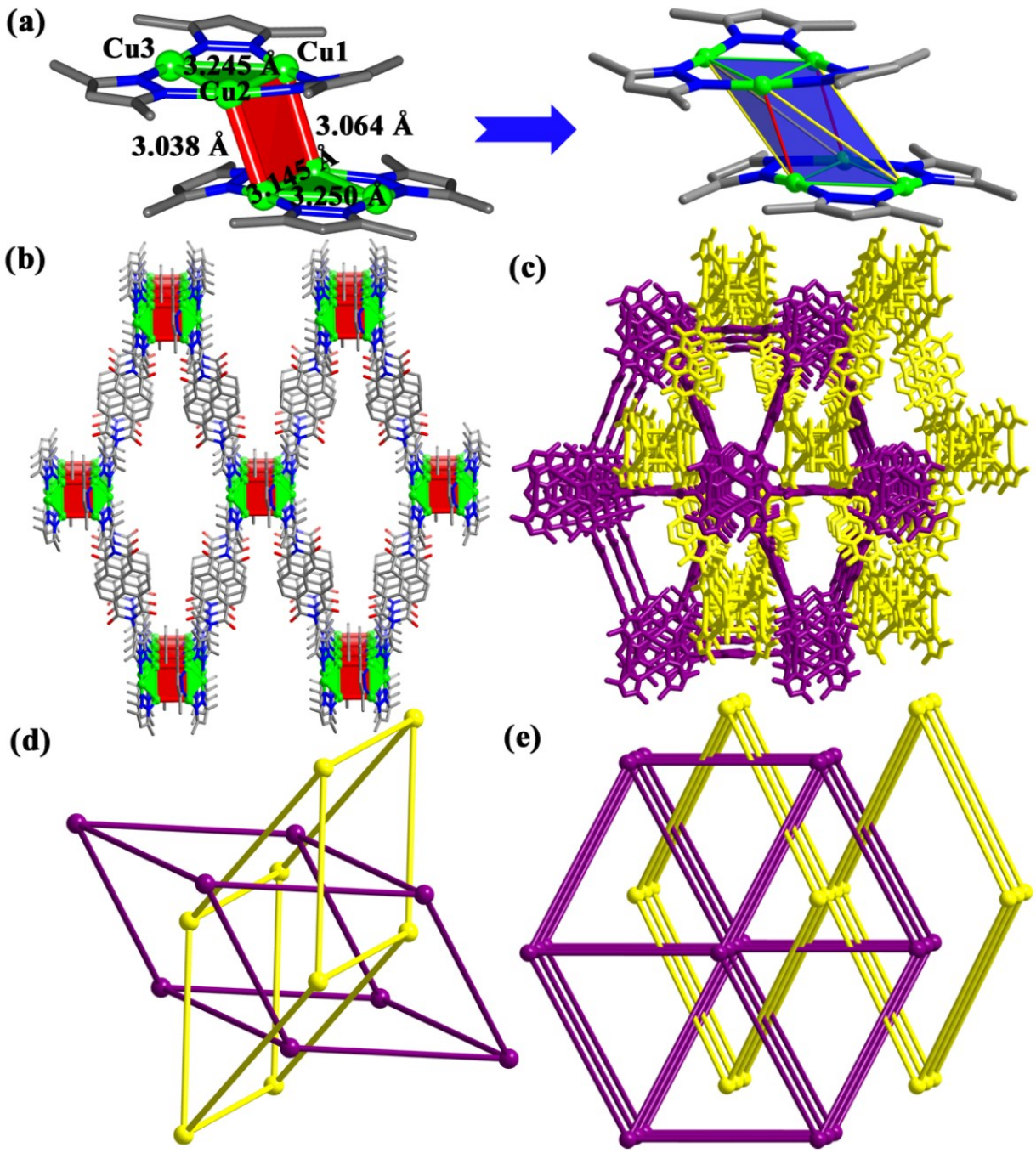

Figure S3 | Schematic representation of the octahedral nodes ($[Cu_6(Pz)_6]$) (a) that are linked by H_2NDI to construct 3D network (b) which interlock together (d) to form a 6-connected ***pcu*** topology (c & e). Color code: Cu, bright green; C, gray; O, red; N, blue. Hydrogen atoms are omitted for clarity.

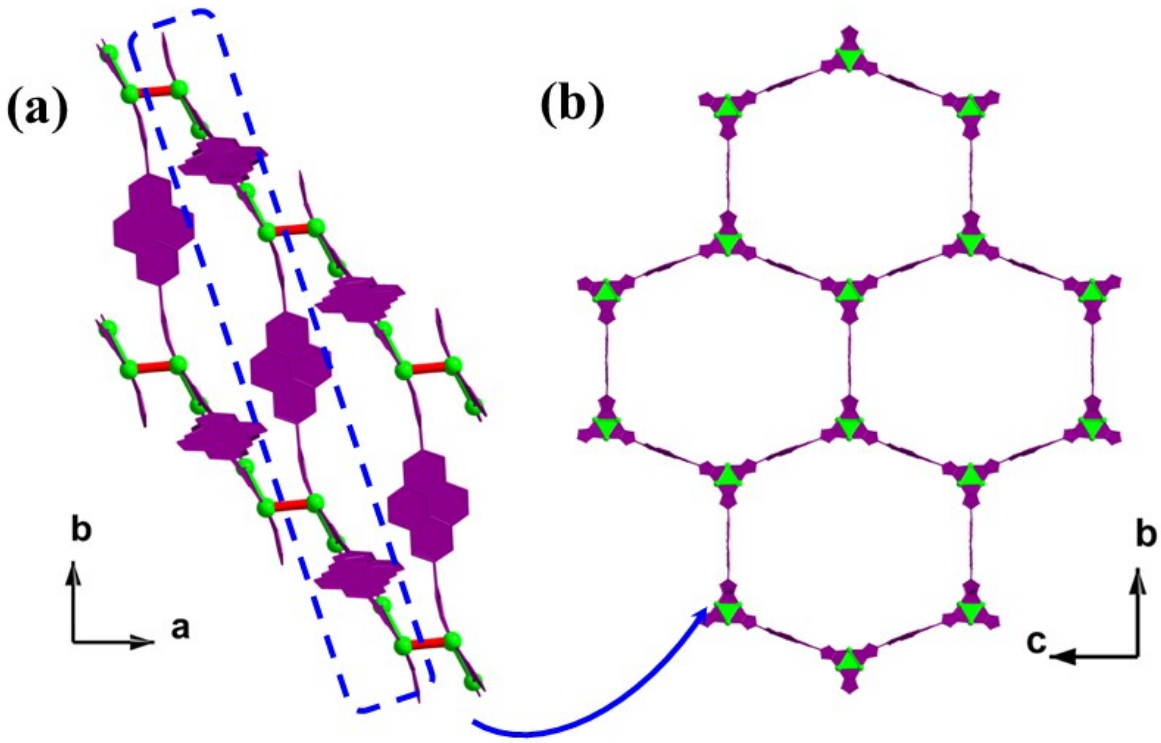

Figure S4 | The intertrimer cuprophilicity (red sticks) makes the adjacent honeycomb layers coupled together to form the 3D network.

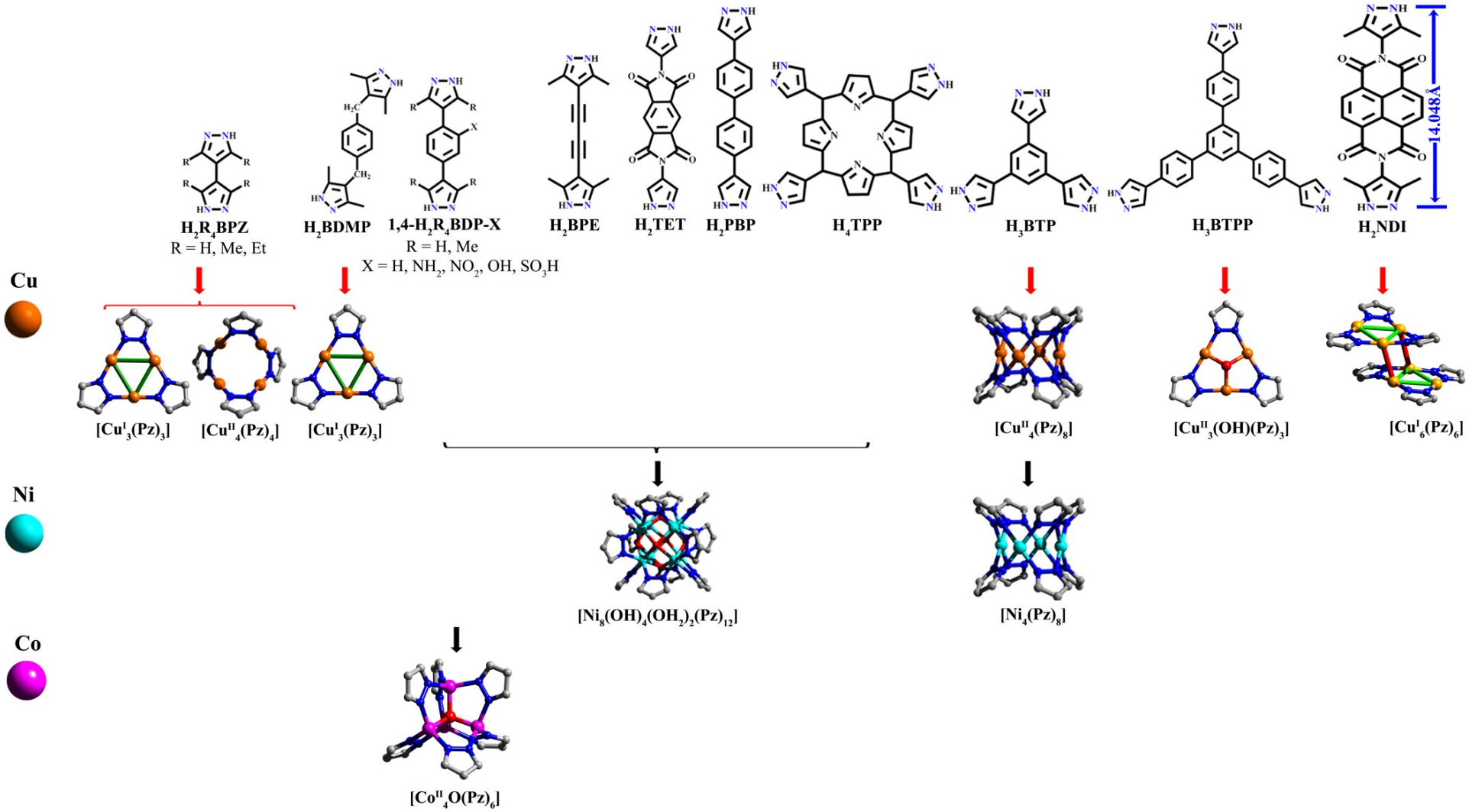

Figure S5 | Schematic representation of various Pz ligands used to construct a subgroup of MOFs with interesting cluster nodes (M= Cu, Ni and Co). Intra- and inter-trimer cuprophilicity are present as green and red sticks, respectively. The stability and fantastic properties for these MOFs are listed in Table. S4.

Computational Methodology.

DFT calculations for two model compounds, $[Cu_3(Pz)_3]$ trimer and $[Cu_6(Pz)_6]$ trimer dimer, were performed at DFT/B3LYP[3] level using *Gaussian03* program.[4] The 6-31G(*d*) basis set was used for C, N and H elements, whereas the Lanl2dz ECP (effective core potential) basis set[5] was used for Cu elements. The geometrical optimization is based on the crystallographic data of $[Cu_6\{3,5\text{-}(CH_3)_2Pz\}_6]$. To simplify the calculation, all methyl substituent groups on the pyrazolate rings are replaced by hydrogen atoms. The molecular structure of $[Cu_6(Pz)_6]$ trimer dimer used for calculation is present below. The Hatree-Fock single-point calculations of $[Cu_3(Pz)_3]$ trimer is -1265.360165 a.u. and $[Cu_6(Pz)_6]$ trimer dimer is -2530.727760 a.u.. Then the energy for the intertrimer cuprophilic interactions (ΔE = +4.66 kcal mol^{-1}) can be obtained, further proving the intertrimer cuprophilicity.[14] The computed gross populations of HOMO and LUMO in the $[Cu_6(Pz)_6]$ trimer dimer are listed in Table S6, while the contours of the frontier orbitals for the $[Cu_6(Pz)_6]$ with single-crystal geometry is shown in Figs. 1g and 1h.

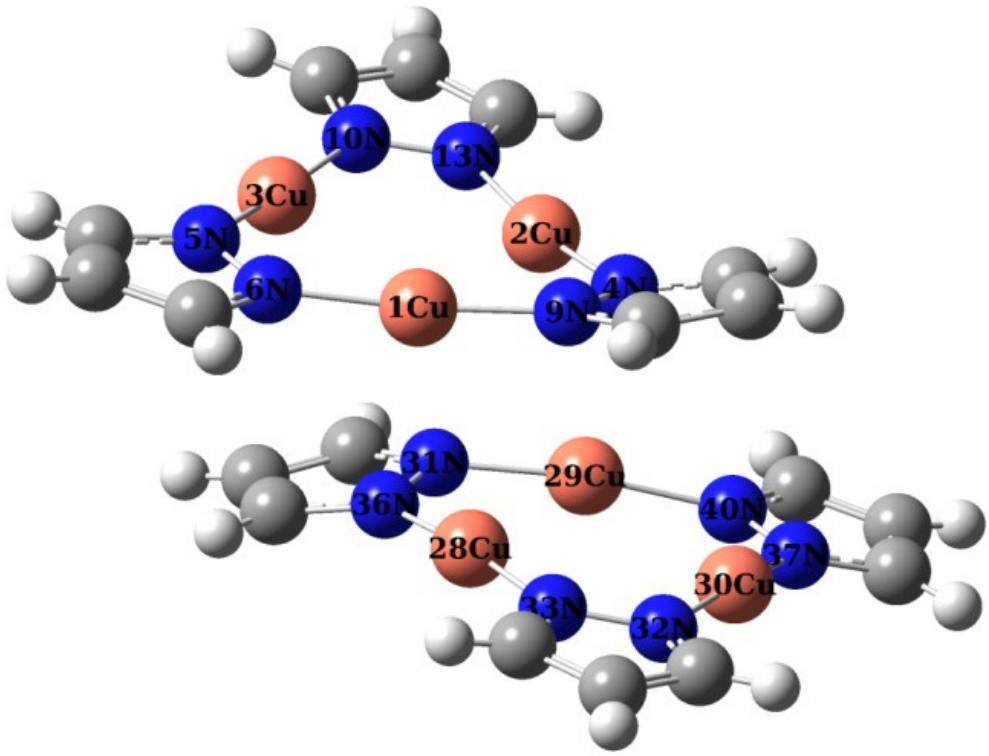

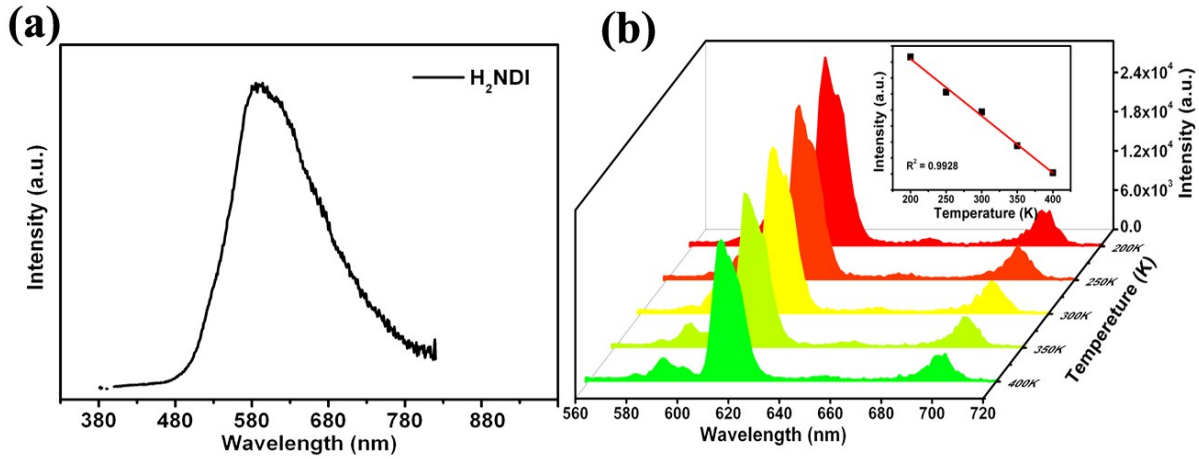

Figure S6 | (a) The fluorescence emission spectra for H_2NDI. (b) Emission spectra of **FJU-66·S** at the temperature range from 200 to 400 K (excited at 345 nm), (Inset) temperature-dependent intensity of cuprophilicity and fitted curves are monitored at 612 nm.

Upon excitation at 345 nm, **FJU-66·S** displays a emission peak at 590 nm which can be assigned to the NDI ligands, while the cuprophilic interactions exhibits emissions at 612 and 698 nm. With decreasing temperature, the emission peak locations of **FJU-66·S** remain unchanged, but the luminescence intensity increases, which may be owing to the gradual cooling limits thermally activated intramolecular rotations and nonradiative-decay.[6-7] The luminescence intensity for **FJU-66·S** shows good linear relationship with the temperature (R^2 = 0.9928), enabling **FJU-66·S** to act as an excellent fluorescence temperature sensor.

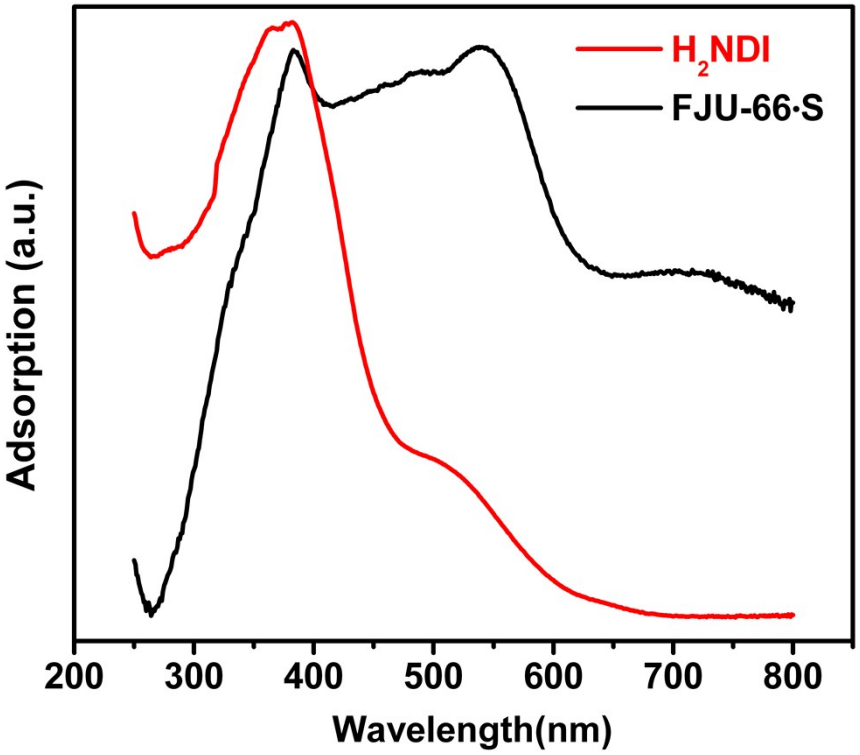

Figure S7 | The comparison of solid-state UV-vis absorption spectra for H_2NDI and **FJU-66·S**.

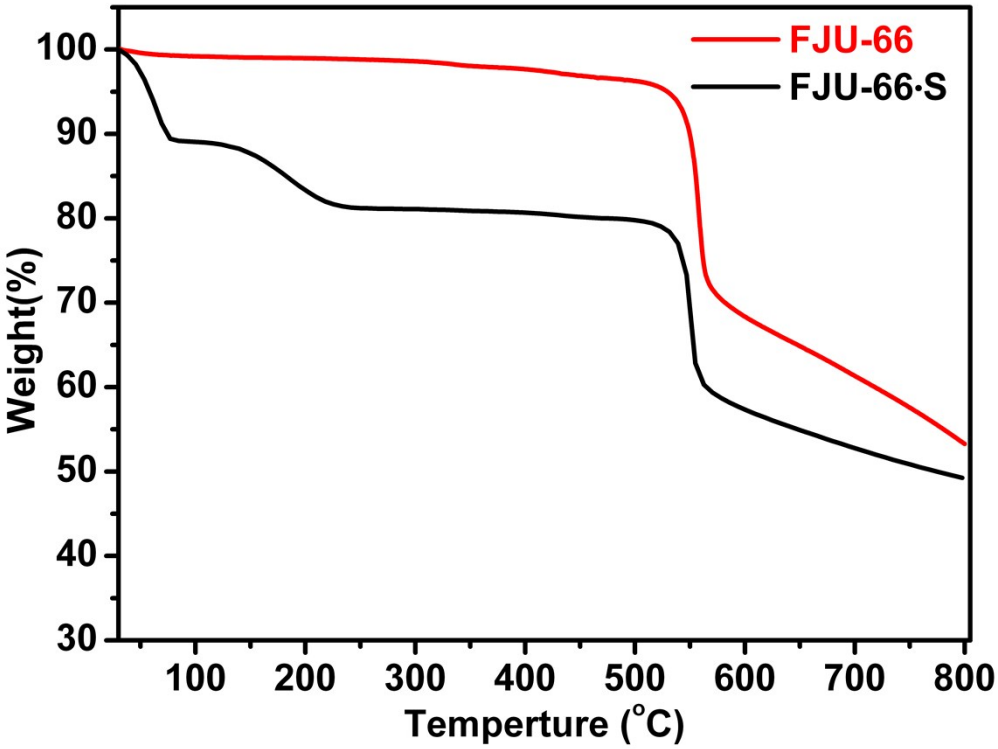

Figure S8 | TGA of **FJU-66·S** and **FJU-66**. From the TGA curves, the as-synthesized and activated samples show a plateau up to 803 K following with sharp weight loss, indicating the collapse of the frameworks.

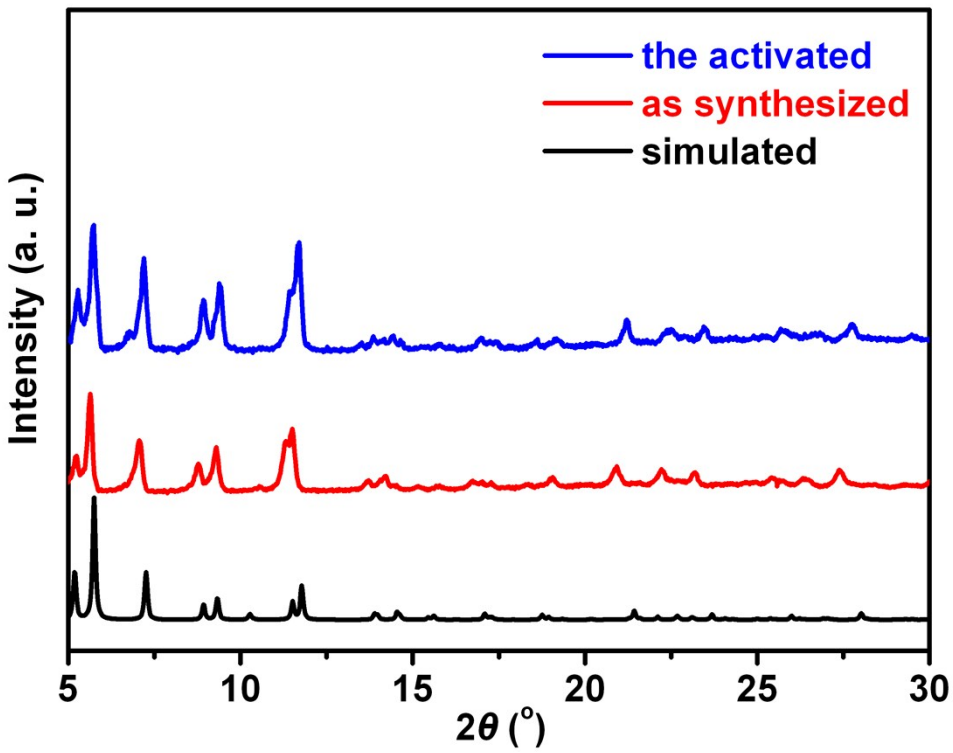

Figure S9 | PXRD patterns of the simulated, as-synthesized and activated **FJU-66·S**. The PXRD pattern of the **FJU-66·S** is coincident with the simulated, indicating a good purity and homogeneity of the compound.

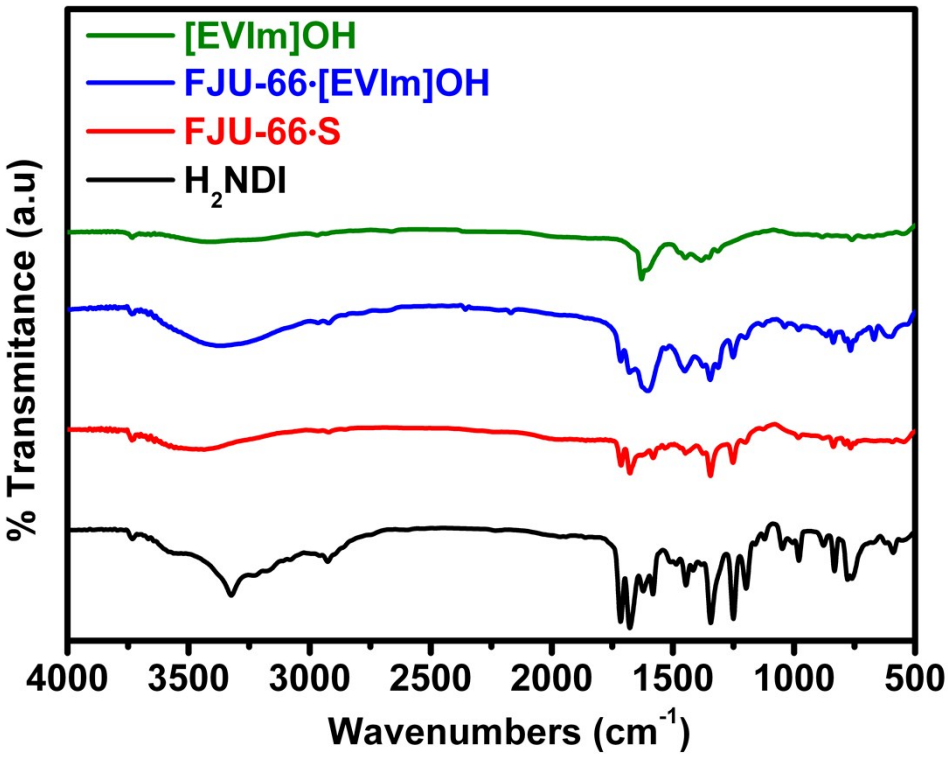

Figure S10 | IR spectrum of H_2NDI, [EVIm]OH, **FJU-66·S** and **FJU-66·[EVIm]OH**.

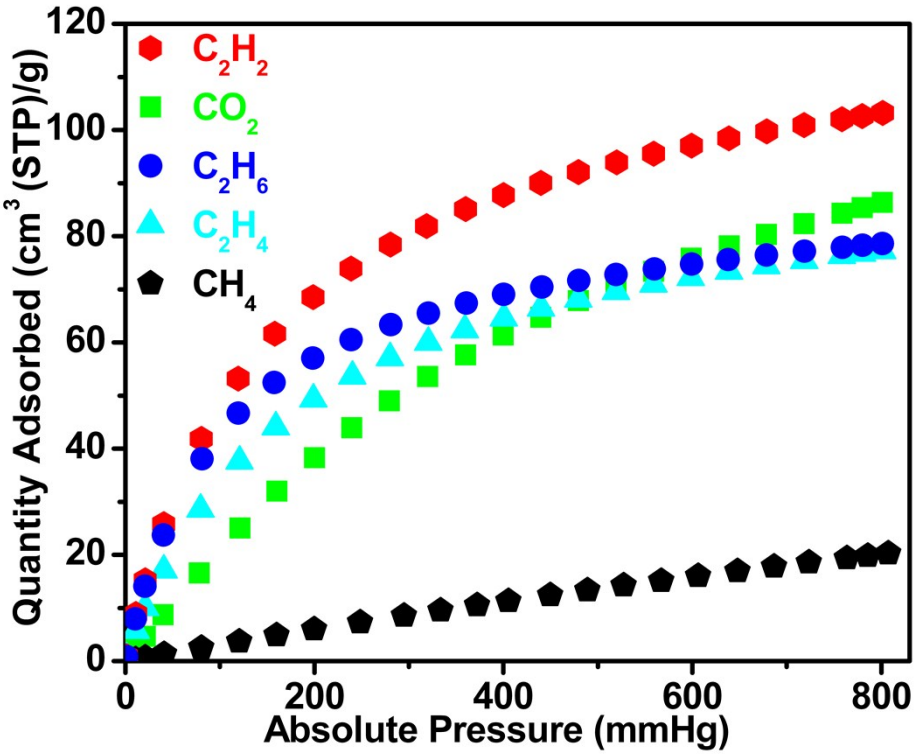

Figure S11 | C_2H_2, C_2H_6, C_2H_4, CO_2, CH_4, and N_2 sorption isotherms of **FJU-66** at 273 K. **FJU-66** takes up differential amount of C_2H_2 (103.2 cm^3/g), C_2H_6 (78.6 cm^3/g), C_2H_4 (77.2 cm^3/g), CO_2 (86.4 cm^3/g), CH_4 (20.3 cm^3/g) and N_2 (5.2 cm^3/g) at 273 K and 1 atm.

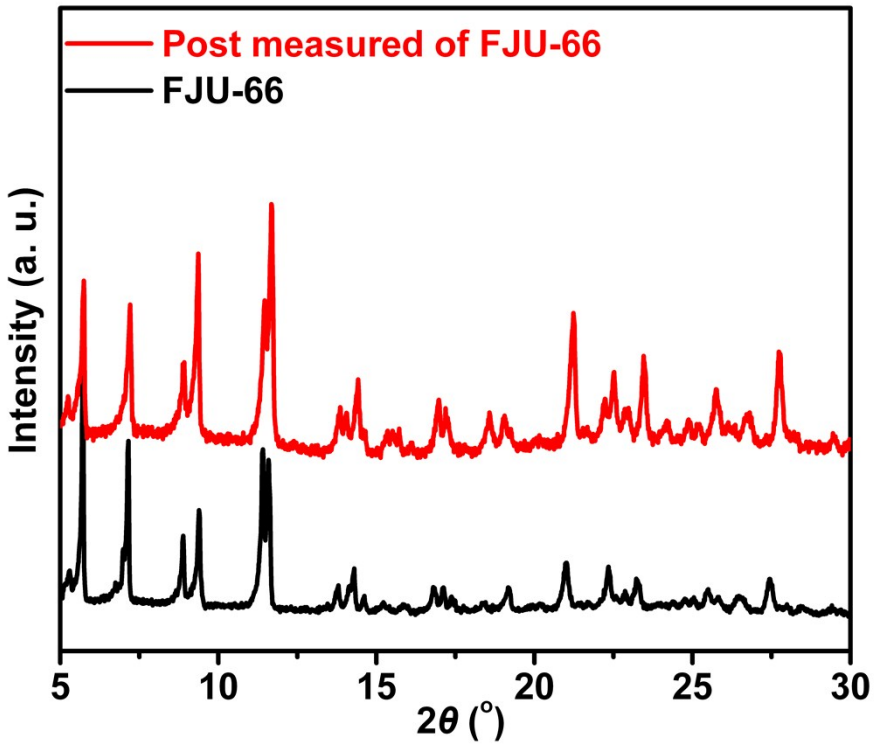

Figure S12 | PXRD patterns of **FJU-66** and post measured samples. The PXRD patterns of **FJU-66** post measured samples remain unchanged which indicated the sample remains structure was retained.

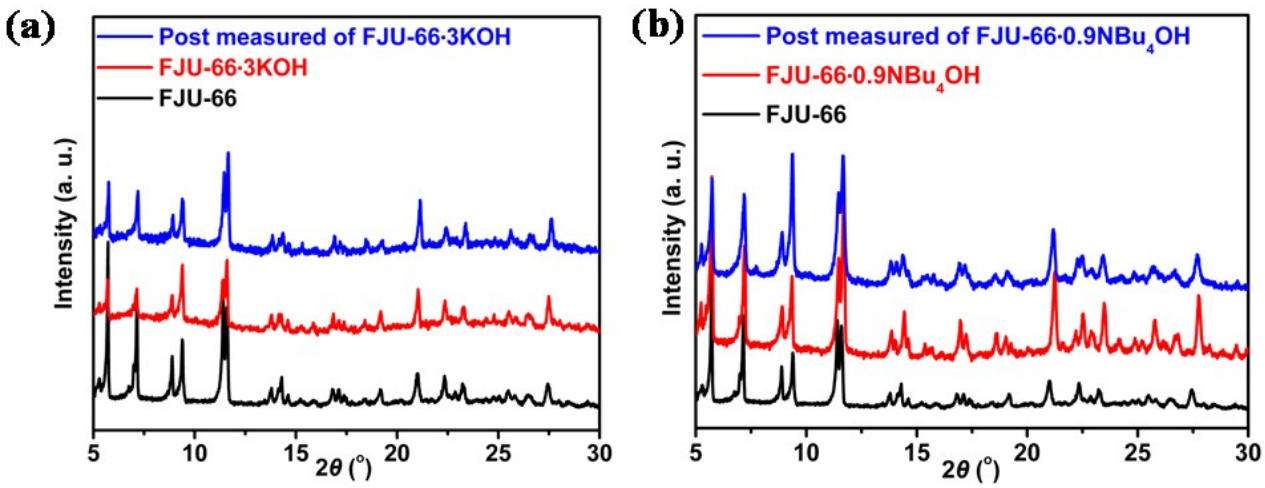

Figure S13 | PXRD patterns of **FJU-66·3KOH**, **FJU-66·0.9NBu$_4$OH** and post measured samples.

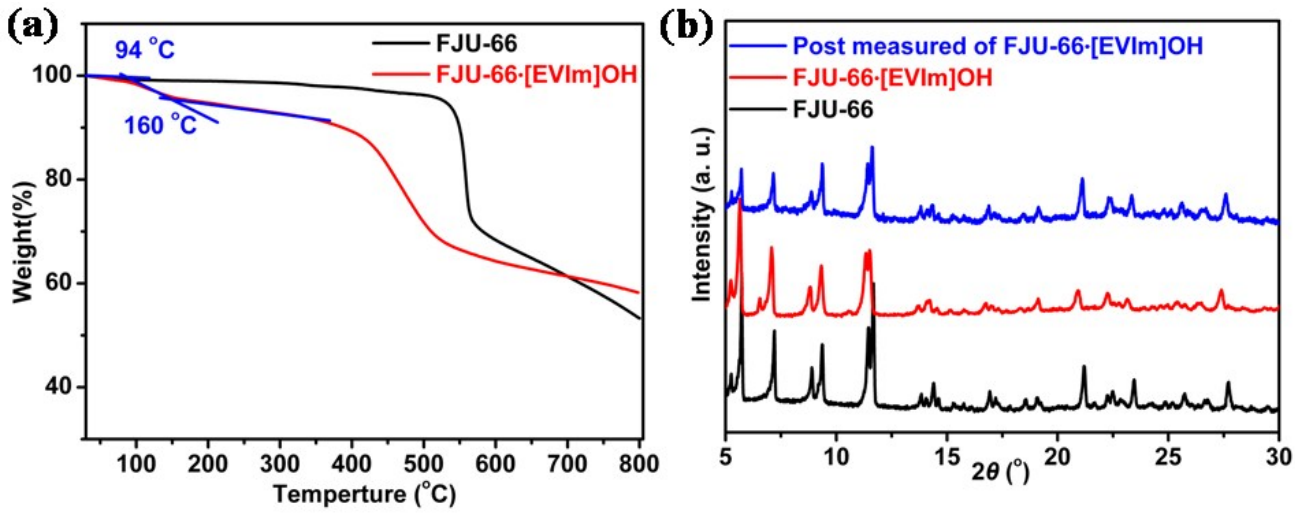

Figure S14 | TGA curves and PXRD patterns of **FJU-66** and **FJU-66·[EVIm]OH**. (a) TGA curves of **FJU-66** (black) and **FJU-66·[EVIm]OH** (red). (b) PXRD patterns of **FJU-66·[EVIm]OH** and post measured samples.

The thermogravimetric profiles show **FJU-66** and **FJU-66·[EVIm]OH** which were all actived at 80 °C overnight in advance. The release of accommodated [EVIm]OH in **FJU-66** starts at 94 °C and finishes at 160 °C. PXRD implying the structures of **FJU-66** remained unchanged after guests being loaded and during the test.

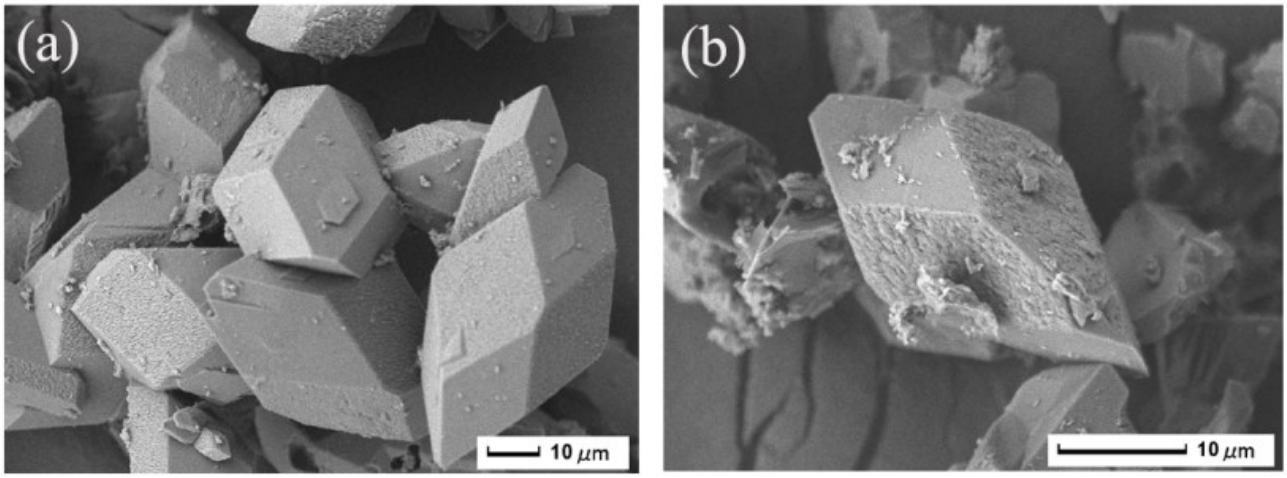

Figure S15 | Scanning electron microscope images of **FJU-66·S** (a) and **FJU-66·[EVIm]OH** (b). There is no obvious change in the surfaces of **FJU-66·[EVIm]OH** in comparison with their own parent materials, indicating [EVIm]OH molecules entered into pores of **FJU-66** frameworks without being aggregated on the outer surface of **FJU-66**.

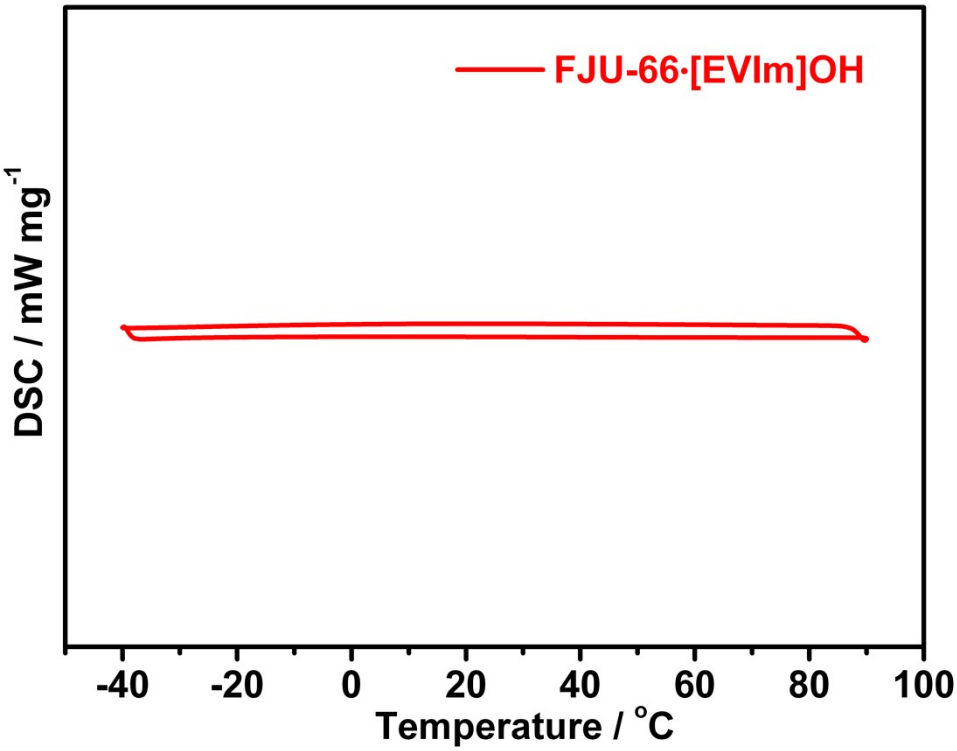

Figure S16 | DSC profiles for **FJU-66·[EVIm]OH**. The measurement was range from -40 to 90 °C, which doesn't present a clear peak, suggesting that no bulk [EVIm]OH is accommodated in the framework.

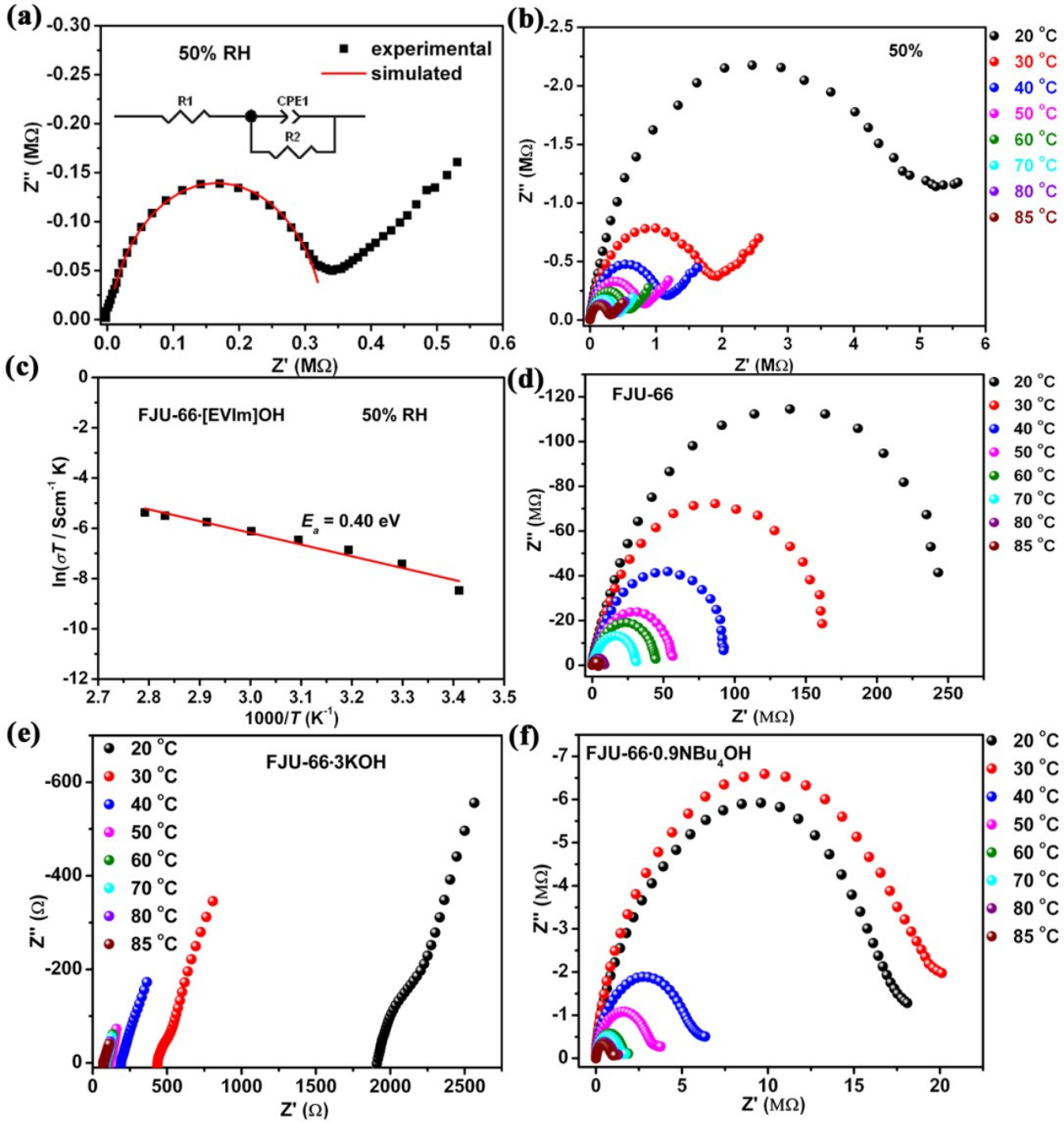

Figure S17 | The Ionic conductivity of **FJU-66**, **FJU-66·[EVIm]OH**, **FJU-66·3KOH** and **FJU-66·0.9NBu$_4$OH**. (a) Nyquist plots for **FJU-66·[EVIm]OH** under 95% RH during the cooling process. (b) Nyquist plots for **FJU-66·[EVIm]OH** under 50% RH at different temperature. (c) Arrhenius plots of 80 °C dependence of conductivity for the studied systems under 50% RH of **FJU-66·[EVIm]OH**. Full symbols represent experimental measurements, and continuous lines the fitting of the data. The inset in (c) represent the equivalent circuit used to analyze the impedance measurements. Nyquist plots for **FJU-66** (d), **FJU-66·3KOH** (e) and **FJU-66·0.9NBu$_4$OH** (f) under 95% RH at different temperature.

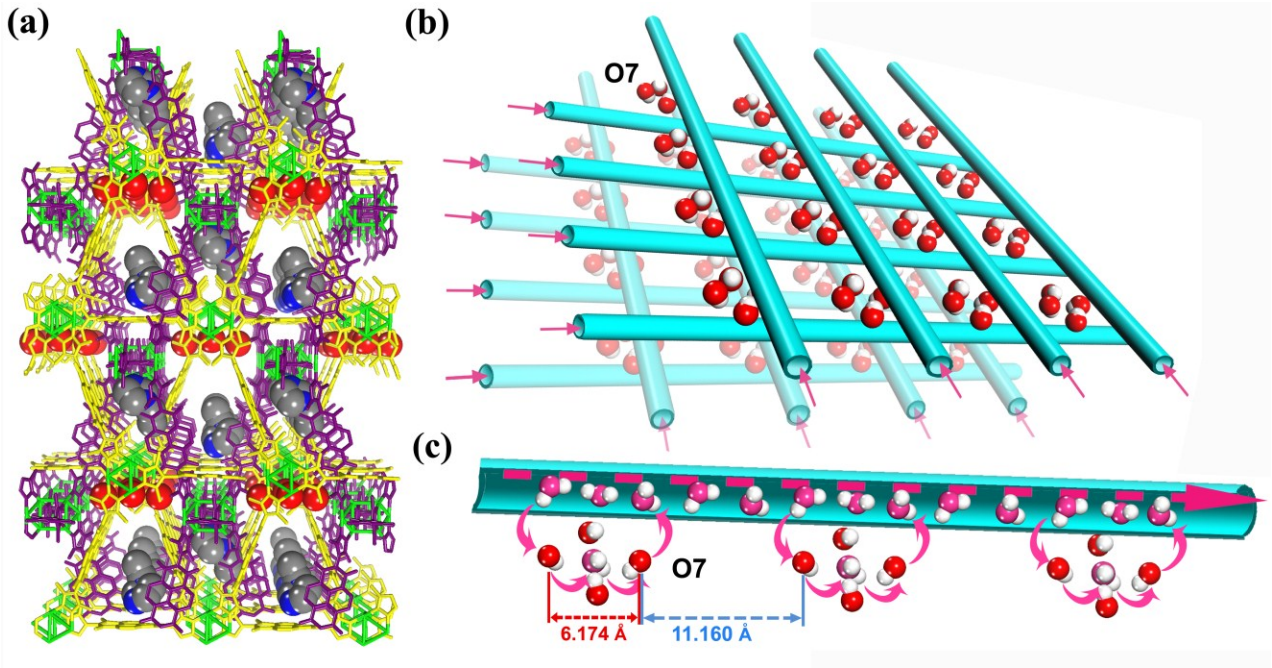

Figure S18 | Ionic transport pathway of **FJU-66·[EVIm]OH**. (a) Packing view of **FJU-66·[EVIm]OH** along the *a* direction. (b) Packing view of the available water pathways along the *a* and *b* directions in **FJU-66**. (c) Possible supramolecular chain formed by hydroxide anions and water molecules inside the channel of **FJU-66** for efficient hydroxide ion conduction. Color code: Cu, bright green; C, gray; O in MOF and hydroxide, red; O in water molecules, pink; N, blue. Hydrogen atoms are omitted for clarity in (a).

Table S1 | Crystal Data and refinement results for the **FJU-66·S**, **FJU-66**, **FJU-66·[EVIm]OH**.

	FJU-66·S	**FJU-66**	**FJU-66·[EVIm]OH**
CCDC	1475870	1475871	1475872
empirical formula	$C_{36}H_{24}Cu_3N_9O_6$	$C_{36}H_{24}Cu_3N_9O_6$	$C_{38.02}H_{25.15}Cu_3N_{9.58}O_{6.29}$
formula weight	869.26	869.26	907.06
Temperature	100 K	100 K	100 K
Radiation	CuKα (λ = 1.54184 Å)	CuKα (λ = 1.54184 Å)	CuKα (λ = 1.54184 Å)
crystal system	tetragonal	tetragonal	tetragonal
space group	*I*-4	*I*-4	*I*-4
Dimensions	3D	3D	3D
a(Å)	17.2079 (3)	17.4696 (5)	17.3245 (3)
b (Å)	17.2079 (3)	17.4696 (5)	17.3245 (3)
c (Å)	34.0361 (10)	33.7023 (9)	33.9396 (6)
α	90°	90°	90°
β	90°	90°	90°
γ	90°	90°	90°
Volume (Å^3)	10078.5 (4)	10285.5 (7)	10186.6 (3)
Z	8	8	8
Density (calcd)	1.146 g/cm^3	1.128 g/cm^3	1.183 g/cm^3
Absorption	1.829 mm^{-1}	1.813 mm^{-1}	1.839 mm^{-1}
Goodness-of-fit on F^2	1.013	1.036	1.033
F(000)	3504.0	3520.0	3659.0
*R*1, *wR*2 [*I*>2*σ*(*I*)][(a)]	0.0561, 0.1215	0.0805, 0.2121	0.0611, 0.1618
*R*1, *wR*2 (all data)[(a)]	0.1121, 0.1426	0.1387, 0.3114	0.0844, 0.1790

(a) $R_1 = \sum ||F_O| - |F_C|| / \sum |F_O|$; $wR_2 = \left[\sum w(|F_O|^2 - |F_C|^2)^2 / \sum w(F_O{}^2)^2\right]^{1/2}$

Table S2 | Selected bond lengths [Å] and bond angles [°] for **FJU-66·S**.

Atom-Atom	bond lengths [Å]	Atom-Atom	bond lengths [Å]
Cu1-Cu1[#1]	3.064 (5)	Cu2 -Cu2	3.038 (3)
Cu1 -N6	1.820 (8)	Cu1 -N1	1.833 (8)
Cu2 -N2	1.817 (8)	Cu2 -N3	1.848 (8)
Cu3 -N5	1.867 (8)	Cu3 -N4	1.865 (9)
Atom-Atom-Atom	**Angle/°**	**Atom-Atom-Atom**	**Angle/°**
N3 -Cu2 -Cu2[#1]	109.5 (3)	N2 -Cu2 -Cu2[#1]	76.3 (3)
N1 -Cu1 -N6	170.3 (5)	N2 -Cu2 -N3	173.4 (4)
N5 -Cu3 -N4	172.7 (4)	C26 -N2 -Cu2	132.7 (8)
N1 -N2 -Cu2	120.2 (7)	N6 -N5 -Cu3	119.8 (6)
C3 -N5 -Cu3	135.5 (8)	N5 -N6 -Cu1	121.8 (9)
C2 -N6 -Cu1	130.9 (10)	N2 -N1 -Cu1	116.6 (7)
C24 -N1 -Cu1	132.3 (8)	N3 -N4 -Cu3	118.8 (6)
C21 -N5 -Cu3	130.3 (8)	N4 -N3 -Cu2	120.8 (6)
C31 -N3 -Cu2	129.3 (12)		

[#1] 1-*x*, 1-y, +*z*

Table S3 | The intra- and intertrimer Cu···Cu distances (Å) and decomposition temperature ($T_{dec,}$ K) for the $[Cu_3(Pz)_3]$-base complexes.

Complexes	Structure Type	Cu···$Cu_{intratrimer}$	Cu···$Cu_{intertrimer}$	T_{dec}	Refs.
FJU-66·S	3D polymer	3.146-3.250	3.038-3.064	803	This work
$\{[Cu(Ppz)]_3[CuCN]_3\}$	3D polymer	3.128-3.249	3.317	-	8
$[Cu_2(Bpz)]_n$	3D polymer	3.022	3.331	668	9
$[Cu_4I_4(NH_3)Cu_3L_3]_n$ (L = 3-(4-pyridyl)-5-p-tolyl-pyrazolate)	2D polymer	3.2104	3.646	663	10
$[(Cu_3I_3)(Cu_3L_3)_2\cdot H_2O]_n$ (L=3-(4-pyridyl)-5-isobutyl-pyrazolate)	chain polymer	2.9867	-	633	11
$[Cu_3\{3\text{-}(CF_3)Pz\}_3]_n$	chain polymer	3.214-3.264	3.100-3.482	-	12
α-$[Cu(Pz)]_n$	chain polymer	3.1653	3.337	-	13
$\{ Cu_3[3\text{-}(CF_3),5\text{-}(Me)Pz]_3\}_n$	chain polymer	3.201-3.245	3.704- 3.915	-	13
$[Cu_3\{3,5\text{-}(CF_3)_2Pz\}_3]_n$	chain polymer	3.221-3.242	3.813–3.987	-	13
$\{ Cu_3[3\text{-}(CF_3),5\text{-}(Ph)Pz]_3\}_n$	chain polymer	3.147-3.258	3.848- 4.636	-	13
$[Cu_3\{2\text{-}(3(5)\text{-}Pz)Py\}_3]_2\cdot 2py$	dimer	3.520	2.905	-	14
$[Cu3(MBPz)_3]_2$	dimer	3.160-3.206	3.135-3.214	-	15
$[Cu_3\{3,5\text{-}(Me)_2,4\text{-}(NO_2)Pz\}_3]_2$	dimer	3.185-3.225	3.329	-	16
$[Cu_3(Ppz)_3]_2$	dimer	3.172-3.230	3.439	-	9
$[Cu_4\{2\text{-}(3(5)\text{-}Pz,6\text{-}(Me)py)\}_4]_2$•3tol	dimer	3.580	3,005	-	17
$\{ Cu_3[3,5\text{-}(Me)_2,4\text{-}(ph)Pz]_3\}_2$	dimer	3.214-3.322	3.580	-	18
$[Cu_3\{3,5\text{-}(Pr^i)_2Pz\}_3]$	monomer	3.191-3.237	-	-	19
$[Cu\{3,5\text{-}(Me)_2Pz\}]_3$	monomer	3.195-3.257	2.946	-	20
$[Cu_6L_3]$ (L=p-xylylene- bis(3,5-dimethyl) pyrazol-4-yl)	monomer	3.174-3.217	3.696-3.946	-	21
$[Cu_6L_3(Cu_2I_2)Cu_6L_3]$ L =3,5-bis ((3,5-dimethyl-pyrazol-4-yl)methyl)-2,6-dimethylpyridine	monomer	3.198-3.212	3.830	-	22

Table S4 | The stability, crystallinity and special features for the representative Pz-base MOFs.

Formula	Abbreviation	Nodes	Crystallinity	Heat Stability (°C)	Chemical (pH) stability	Special Features	Refs.
$[Cu_6(NDI)_3 \cdot 2DMF \cdot 6MeOH \cdot 2H_2O]$	**FJU-66·S**	$[Cu_6(Pz)_6]$	crystal	530	1mM HCl-10M NaOH	Fluorescence temperature sensing, ultrastability and high hydroxide – ionic conductivity	This work
$Zn_3(BTP)_2 \cdot 4CH_3OH \cdot 2H_2O$	$Zn_3(BTP)_2$	infinite Zn chain	microcrystal	510	-	High thermal and chemical stability	23
$Zn(1,3\text{-}BDP) \cdot 0.7DMF \cdot 0.5H_2O$	Zn(1,3-BDP)	infinite Zn chain	powder	500	-	Hydrogen storage	24
Zn(NDI-X)	Zn(NDI-X)	infinite Zn chain	powder	500	-	Modulate water adsorption processes; Electrochromism	2
$[Cu_2(phbpz)] \cdot 2DEF \cdot MeOH$	CFA-2	$[Cu_3(Pz)_3]$	crystal	500	-	High thermal stability	25
α-$[Cu_2(bpz)]$		$[Cu_3(Pz)_3]$	crystal	500	-	Guest-uptake	26
β-$[Cu_2(bpz)]$		$[Cu_3(Pz)_3]$	crystal	500	-	Guest-uptake	27
$Ni_3(BTP)_2 \cdot 3CH_3OH \cdot 10H_2O$	$Ni_3(BTP)_2$	$[Ni_4(Pz)_8]$	microcrystal	450	2-14	High thermal and chemical stability	24
$Co_3(BTP)_2 \cdot 8CH_3OH \cdot 10H_2O$	$Co_3(BTP)_2$	infinite Co chain	microcrystal	450	-	High thermal and chemical stability	24
Ni(bpb)	Ni(bpb)	infinite Ni chain	powder	450	-	Adsorption of harmful organic vapors	27
[Ni(BPEB)]	[Ni(BPEB)]	infinite Ni chain	powder	422	-	Gas adsorption	28

$Co(BDP)\cdot 2DEF\cdot H_2O$	Co(BDP)	infinite Co chain	crystal	420	-	Broadly hysteretic H_2 adsorption	29
$[Fe_2(BPEB)_3]$	$[Fe_2(BPEB)_3]$	infinite Fe chain	powder	415	5-9	Gas adsorption	29
[Zn(BPEB)]	[Zn(BPEB)]	infinite Zn chain	powder	410	-	Gas adsorption	29
$[Ni_8(OH)_4(OH_2)_2(\mu_4\text{-}L)_6]\cdot nH_2O$		$[Ni_8(OH)_4(H_2O)_2(Pz)_{12}]$	powder	410	-	High porosity	30
$Zn(1,4\text{-}BDP)\cdot 2DEF\cdot H_2O$		infinite Zn chain	powder	400	-	Hydrogen storage	25
$Cu_3(BTP)_2\cdot 8CH_3OH\cdot 10H_2O$	$Cu_3(BTP)_2$	$[Cu_4(Pz)_8]$	microcrystal	390	3-14	High thermal and chemical stability	24
$[Ni_8(OH)_4(H_2O)_2(L)_6]_n$		$[Ni_8(OH)_4(H_2O)_2(Pz)_{12}]$	powder	350	-	Capture of harmful volatile organic compounds	31
α-$[Ag_2(bpz)]$		$[Ag_3(Pz)_3]$	crystal	350	-	Guest-uptake	27
$[Ni_8(OH)_4(OH_2)_2$ (4,40-(buta-1,3-diyne-1,4-diyl) bispyrazolato)$_6]_n$		$[Ni_8(OH)_4(H_2O)_2(Pz)_{12}]$	microcrystal	340	-	Incorporation and release of drug	32
$Cu(Me_4BPz)$		$[Cu_4(Pz)_4]$	powder	310	-	Gas adsorption	33
$[Ni_8(OH)_4(H_2O)_2(TPP)_3]$	PCN-601	$[Ni_8(OH)_4(H_2O)_2(Pz)_{12}]$	microcrystal	300	0.1mM HCl-20M NaOH	Extraordinary base-resistance	34
β-$[Ag_2(bpz)]$		$[Ag_3(Pz)_3]$	crystal	300	-	Guest-uptake	27
$[Ag_2(phbpz)]$	CFA-3	$[Ag_3(Pz)_3]$	crystal	300	-	High thermal stability	26
$[Co^{II}_4O(bdpb)_3]$	MFU-1	$[Co_4O(Pz)_6]$	microcrystal	270	-	Heterogeneous catalytic oxidation	35

Table S5 | The value of the bond valence sums (V_i) for **FJU-66·S**.

Cu1		
Bond	d_{ij}(Å)	V_{ij}
Cu1 -N1	1.833	0.547
Cu1 -N6	1.820	0.567
	V_i	1.114
Cu2		
Cu2 -N2	1.817	0.572
Cu2 -N3	1.848	0.526
	V_i	1.098
Cu3		
Cu3 -N4	1.865	0.502
Cu3 -N5	1.867	0.499
	V_i	1.001

Here the valence $V_{ij} = e^{[\frac{R_0 - d_{ij}}{B}]}$ and $V_i = \pm \sum_j V_{ij}$. D_{ij} is the bond length between the two ions. R_0 is the reference bond length with 1.61 Å for Cu-N bond. B is a constant approximately equal to 0.37 Å.

The values of the bond valence sums (V_i) for the three crystallographically independent copper ions are 1.114, 1.098 and 1.001, respectively, close to the value for the monovalent ion.

Table S6 | The computed gross populations of HOMO and LUMO in $[Cu_6(Pz)_6]$ trimer dimer.

HOMO

	7XX	7YY	7ZZ	7XY	7XZ	7YZ		3S	3PX	3PY	3PZ
Cu1	-0.12294	0.05034	0.07616	0.16627	-0.16209	0.07756	N4	-0.09820	-0.04225	-0.03234	-0.07678
Cu2	0.19941	-0.03668	-0.16773	0.27411	0.20774	0.09992	N5	-0.02141	-0.00024	-0.00616	0.01107
Cu3	0.03212	-0.04618	0.01475	-0.03184	0.00549	0.02023	N6	0.02714	-0.03884	0.02468	0.00285
Cu28	0.12287	-0.05031	-0.07613	0.16612	0.16194	0.07747	N9	0.08908	0.03810	-0.01765	0.05333
Cu29	-0.19928	0.03657	0.16771	0.27395	-0.20757	0.09975	N10	0.03419	-0.00173	-0.03110	-0.01324
Cu30	-0.03203	0.04600	-0.01465	-0.03178	-0.00548	0.02013	N13	-0.04300	0.07203	0.04099	-0.01991
							N31	0.09817	-0.04216	0.03233	-0.07679
							N32	0.02141	-0.00021	0.00620	0.01102
							N33	-0.02718	-0.03883	-0.02467	0.00278
							N36	-0.08904	0.03808	0.01762	0.05325
							N37	-0.03416	-0.00173	0.03105	-0.01322
							N40	0.04298	0.07197	-0.04096	-0.01989

LUMO

	3S	5PX	5PY	5PZ	6PX	6PY	6PZ		3S	3PX	3PY	3PZ
Cu1	-0.13596	0.19509	0.16127	-0.11424	0.10366	0.24980	0.19503	N4	-0.09287	-0.09005	0.00748	0.08768
Cu2	-0.15625	0.08478	-0.08292	0.09265	-0.06022	-0.15301	-0.06091	N5	-0.11102	-0.01320	0.01531	0.06671
Cu3	-0.16108	-0.07473	0.00247	-0.04218	-0.10978	-0.05521	-0.11679	N6	0.04090	0.02135	0.00198	-0.02391
Cu28	-0.13557	-0.19521	0.16156	0.11427	-0.10381	0.24988	-0.19494	N9	0.03446	0.08880	0.00951	-0.07940
Cu29	-0.15656	-0.08493	-0.08320	-0.09269	0.06004	-0.15308	0.06090	N10	-0.04255	0.00343	-0.01264	-0.01958
Cu30	-0.16120	0.07504	0.00247	0.04232	0.11000	-0.05524	0.11694	N13	-0.02182	0.01173	0.01166	0.02786
								N31	-0.09294	0.09013	0.00742	-0.08777
								N32	-0.11122	0.01324	0.01525	-0.06680
								N33	0.04060	-0.02148	0.00194	0.02391
								N36	0.03415	-0.08870	0.00951	0.07946
								N37	-0.04270	-0.00342	-0.01256	0.01960
								N40	-0.02202	-0.01176	0.01169	-0.02789

Table S7 | The comparison of thermal stability and chemical stability on **FJU-66·S** with some representative MOFs from the varied-temperature PXRD and/or TGA.

Compounds	Thermal stability(K)	Methods	Refs.	Compounds	Chemical (pH) stability	Refs.
ZIF-8	823	PXRD	36	PCN-601	4 – 14, 20M NaOH	35
FJU-66·S	803	PXRD&TGA	This work	**FJU-66·S**	3 – 14, 10M NaOH	This work
UiO(bpdc)	785	TGA	37	ZIF-8	7 – 14, 8M NaOH	37
Zn_3(BTP)	783	PXRD	24	UiO-66	1 – 14	38
UiO-66	773	TGA	39	$Ni(BTP)_2$	2 – 14	24
Zn(NDI-SOEt)	773	TGA	2	MIL-53	2 – 14	40
CFA-2	773	PXRD	26	Cu_3(BTP)	3 – 14	24
MIL-110	723	TGA	41	PCN-426-Cr	4M HCl, 0 – 12	42
PCN-56	673	TGA	43	PCN-225	1 – 11	49
MIL-100	673	TGA	44	PCN-56	2 – 11	44
$[Cu_2(BPz)]_n$	668	TGA	10	PCN-600 (Fe)	2 – 11	45
MIL-53	648	PXRD	46	UiO-66-NH_2	1 – 9	47
PCN-225	623	TGA	48	$Fe_2(BPEB)_3$	5 – 9	49
MIL-101	623	TGA	50	Cu-BTTri	3 – 7.5	50
PCN-601	573	TGA	35	DUT-69	0 – 7	50
MIL-88	573	PXRD	51	DUT-67	conc. HCl, 0 – 7	50
				MIL-100	0 – 4	45
				PCN-222	2M-8M HCl	52

Table S8 | ICP-AES data for **FJU-66·3KOH.**

Cu (%)	K (%)	Cu : K
4.61	14.02	2.07 : 1

ICP analysis was performed to gauge relative contents of K and Cu reveal that the K/Cu ratio is 1.00 : 2.07 which is in good agreement with the elemental analysis

Supplementary References

1 J. G. Li, J. Gao, H. Li, X. F. Yang and Y. Liu, *Anal. Methods,* 2014, **6,** 4305–4311.

2 (a) C. R. Wade, T. C. Sanchez, T. C. Narayan and M. Dincă, *Energy Environ. Sci.*, 2013, **6,** 2172–2177; (b) C. R. Wade, M. Li and M. Dincă, *Angew. Chem. Int. Ed*., 2013, **52,** 13377–13381.

3 A. D. Becke, J. Chem. Phys., 1993, **98,** 5648–5652.

4 M. J. Frisch, *et al*. GAUSSIAN 03, *Gaussian, Inc*., 2003, Pittsburgh PA.

5 T. R. Cundari, W. J. Stevens and S. O. Sommerer,, *J. Chem. Phys.,* 1993, **98,** 5555–5565.

6 Y. J. Cui, Y. F. Yue, G. D. Qian and B. L. Chen, *Chem. Rev.,* 2012, **112,** 1126–1162.

7 F. Y. Yi, D. X. Chen, M. K. Wu, L. Han and H. L. Jiang, *ChemPlusChem.,* 2016, **81,** 675–690.

8 J. X. Zhang, J.He, Y. G.Yin, M. H. Hu, D. Li and X. C. Huang, *Inorg. Chem.,* 2008, **47,** 3471–3473.

9 J. He, Y. G. Yin, T. Wu, D. Li and X. C. Huang, *Chem. Commun.,* 2006, 2845–2847.

10 S. Z. Zhan, M. Li, X. P. Zhou, J. H. Wang, J. R. Yang and D. Li, *Chem. Commun.,* 2011, **47,** 12441–12443.

11 S. Z. Zhan, M. Li, X. P. Zhou, D. Li and S. W. Ng, *RSC Adv.,* 2011, **1,** 1457–1459.

12 H. V. R. Dias, H. V. K. Diyabalanage, M. G. Eldabaja, O. Elbjeirami, M. A. Rawashdeh-Omary and M. A. Omary, *J. Am. Chem. Soc.,* 2005, **127,** 7489–7501.

13 N. Masciocchi, M. Moret, P. Cairati, A. Sironi, G. A. Ardizzoia and G. L. Monica, *J. Am. Chem. Soc.,* 1994, **116,** 7668–7676.

14 K. Singh, J. R. Long and P. Stavropoulos, *J. Am. Chem. Soc.,* 1997, **119,** 2942–2943.

15 Q. Xiao, J. Zheng, M. Li, S. Z. Zhan, J. H. Wang and D. Li, *Inorg. Chem.,* 2014, **53,** 11604–11615.

16 G. A. Ardizzoia, S. Cenini, G. La Monica, N. Masciocchi, A. Maspero and M. Moret, *Inorg. Chem.,* 1998, **37,** 4284–4292.

17 K. Singh, J. R. Long and P. Stavropoulos, *Inorg. Chem.,* 1998, **37,** 1073–1079.

18 F. Gong, Q. Wang, J. Chen, Z. Yang, M. Liu, S. Li and G. Yang, *Inorg. Chem.,* 2010, **49,** 1658–1666.

19 K. Fujisawa, Y. Ishikawa, Y. Miyashita and K. I. Okamoto, *Chem. Lett.,* 2004, **33,** 66–67.

20 M. K. Ehlert, S. J. Rettig, A. Storr, R. C. Thompson and J. Trotter, *Can. J. Chem.,* 1990, **68,** 1444–1449.

21 G. F. Gao, M. Li, S. Z. Zhan, Z. Lv, G. H. Chen and D. Li, *Chem. Eur. J.,* 2011, **17,** 4113–4117.

22 J. H. Wang, M. Li, J. Zheng, X. C. Huang and D. Li, *Chem. Commun.,* 2014, **50,** 9115–9118.

23 V. Colombo, S. Galli, H. J. Choi, G. D. Han, A. Maspero, G. Palmisano, N. Masciocchic and J. R. Long, *Chem. Sci.,* 2011, **2,** 1311–1319.

24 H. J. Choi, M. Dincă, A. Dailly and J. R. Long, *Energy Environ. Sci.,* 2010, **3,** 117–123.

25 M. Grzywa, C. Geßner, D. Denysenko, B. Bredenkötter, F. Gschwind, K. M. Fromm, W.

Nitek, E. Klemmb and D. Volkmer, *Dalton Trans.,* 2013, **42,** 6909–6921.
26 J. P. Zhang and S. Kitagawa, *J. Am. Chem. Soc.,* 2008, **130,** 907–917.
27 S. Galli, N. Masciocchi, V. Colombo, A. Maspero, G. Palmisano, F. J. López-Garzón, M. Domingo-García, I. F. andez-Morales, E. Barea and J. A. R. Navarro, *Chem. Mater.,* 2010, **22,** 1664–1672.
28 S. Galli, A. Maspero, C. Giacobbe, G. Palmisano, L. Nardo, A. Comotti, I. Bassanetti, P. Sozzanic and N. Masciocchi, *J. Mater. Chem. A,* 2014, **2,** 12208–12221.
29 H. J. Choi, M. Dincă and J. R. Long, *J. Am. Chem. Soc.,* 2008, **130,** 7848–7850.
30 N. Masciocchi, S. Galli, V. Colombo, A. Maspero, G. Palmisano, B. Seyyedi, C. Lamberti and S. Bordiga, *J. Am. Chem. Soc*., 2010, **132,** 7902–7904.
31 N. M. Padial, E. Q. Procopio, C. Montoro, E. López, J. E. Oltra, V. Colombo, A. Maspero, N. Masciocchi, S. Galli, I. Senkovska, S. Kaskel, E. Barea and J. A. R. Navarro, *Angew. Chem. Int. Ed.,* 2013, **52,** 8290–8294.
32 E. Q. Procopio, S. Rojas, N. M. Padial, S. Galli, N. Masciocchi, F. Linares, D. Miguel, J. E. Oltra, J. A. R. Navarro and E. Barea, *Chem. Commun.,* 2011, **47,** 11751–11753.
33 A. Tăbăcaru, C. Pettinari, I. Timokhin, F. Marchetti, F. Carrasco-Marín, F. J. Maldonado-Hódar, S. Galli and N. Masciocchi, *Cryst. Growth Des.,* 2013, **13,** 3087–3097.
34 K. Wang, X. L. Lv, D. Feng, J. Li, S. Chen, J. Sun, L. Song, Y. Xie, J. R. Li and H. C. Zhou, *J. Am. Chem. Soc.,* 2016, **138,** 914−919.
35 M. Tonigold, Y. Lu, B. Bredenkötter, B. Rieger, S. Bahnmüller, J. Hitzbleck, G. Langstein and D. Volkmer, *Angew. Chem. Int. Ed.,* 2009, **48,** 7546-7550.
36 K. S. Park, Z. Ni, A. P. Côté, J. Y. Choi, R. Huang, F. J. Uribe-Romo, H. K. Chae, M. O'Keeffe and O. M. Yaghi, *PNAS.,* 2006, **103,** 10186–10191.
37 L. Li, S. Tang, C. Wang, X. Lv, M. Jiang, H. Wua and X. Zhao, *Chem. Commun.,* 2014, **50,** 2304–2307.
38 C. G. Piscopo, A. Polyzoidis, M. Schwarzer and S. Loebbecke, *MicroporousMesoporous Mater.,* 2015, **208,** 30–35.
39 M. Kandiah, M. H. Nilsen, S. Usseglio, S. Jakobsen, U. Olsbye, M. Tilset, C. Larabi, E. A. Quadrelli, F. Bonino and K. P. Lillerud, *Chem. Mater.,* 2010, **22,** 6632–6640.
40 X. Qian, B. Yadian, R. Wu, Y. Long, K. Zhou, B. Zhu and Y. Huang, *Int. J. Hydrogen Energy.,* 2013, **38,** 16710–16715.
41 M. Haouas, C. Volkringer, T. Loiseau, G. Férey and F. Taulelle, *Chem. Eur. J.,* 2009, **15,** 3139–3146.
42 T. F. Liu, L. F. Zou, D. W. Feng, Y. P. Chen, S. Fordham, X. Wang, Y. Y. Liu and H. C. Zhou, *J. Am. Chem. Soc.,* 2014, **136,** 7813−7816.
43 H. L. Jiang, D. Feng, T. F. Liu, J. R. Li and H. C. Zhou, *J. Am. Chem. Soc.,* 2012, **134,** 14690–14693.
44 G. Férey, C. Serre, C. M. Draznieks, F. Millange, S. Surblé, J. Dutour and I. Margiolaki, *Angew. Chem.,* 2004, **116,** 6456–6461.
45 K. Wang, D. Feng, T. F. Liu, J. Su, S. Yuan, Y. P. Chen, M. Bosch, X. Zou and H. C. Zhou, *J. Am. Chem. Soc.,* 2014, **136,** 13983–13986.

46 C. Serre, F. Millange, C. Thouvenot, M. Noguès, G. Marsolier, D. Louër and G. Férey, *J. Am. Chem. Soc.,* 2002, **124,** 13519–13526.
47 J. Aguilera-Sigalat and D. Bradshaw, *Chem. Commun.,* 2014, **50,** 4711–4713.
48 H. L. Jiang, D. Feng, K. Wang, Z. Y. Gu, Z. Wei, Y. P. Chen and H. C. Zhou, *J. Am. Chem. Soc.,* 2013, **135,** 13934–13938.
49 A. J. Howarth, Y. Y. Liu, P. Li, Z. Y. Li, T. C. Wang, J. T. Hupp1 and O. K. Farha, *Nature Reviews Materials.,* 2016, **1,** 15018−15033.
50 P. Chowdhury, C. Bikkina and S. Gumma, *J. Phys. Chem. C,* 2009, **113,** 6616–6621.
51 S. Surblé, C. Serre, C. Mellot-Draznieks, F. Millangea and G. Féreya, *Chem. Commun.,* 2006, 284–286.
52 D. Feng, Z. Y. Gu, J. R. Li, H. L. Jiang, Z. Wei and H. C. Zhou, *Angew. Chem. Int. Ed*., 2012, **124,** 10453–10456.